RADIO-FREQUENCY OCCULTATIONS AND THE LOW-DEGREE SHAPE OF MERCURY. Mark E. Perry[1], Gregory A. Neumann[2], Catherine L. Johnson[3,4], Roger J. Phillips[5,6], Carolyn M. Ernst[1], Sean C. Solomon[7,8], Jean-Luc Margot[9], Jürgen Oberst[10], Steven A. Hauck, II[11], Maria T. Zuber[12], David E. Smith[12]. [1]The Johns Hopkins Univ. Applied Physics Lab., Laurel, MD 20723, USA (mark.perry@jhuapl.edu). [2]NASA Goddard Space Flight Center, Greenbelt, MD, USA. [3]Dept. of Earth, Ocean and Atmospheric Sciences, Univ. of British Columbia, Vancouver, BC, V6T 1Z4, Canada. [4]Planetary Science Institute, Tucson, AZ 85712, USA. [5]Planetary Science Directorate, Southwest Research Institute, Boulder, CO 80302, USA. [6]Dept. Earth & Planetary Sciences, Washington Univ., St Louis, MO 63130, USA. [7]Lamont-Doherty Earth Observatory, Columbia Univ., Palisades, NY 10964, USA. [8]Dept. of Terrestrial Magnetism, Carnegie Institution of Washington, Washington, DC 20015, USA. [9]Dept. of Earth, Planetary, and Space Sciences, Univ. of California, Los Angeles, CA 90095, USA. [10]German Aerospace Center, Institute of Planetary Research, Berlin, Germany. [11]Dept. of Earth, Environmental, and Planetary Sciences, Case Western Reserve Univ., Cleveland, OH 44106, USA. [12]Dept. of Earth, Atmospheric and Planetary Sciences, Massachusetts Institute of Technology, Cambridge, MA 02139, USA.

Introduction: The degree to which Mercury's shape deviates from a sphere provides insight into the mantle density, lithosphere stiffness, global distribution of crust, and thermal and spin-state history that led to the current state of these properties. The best constraints on these parameters are inferred from comparisons of Mercury's shape to its geoid [1]. Some 25 million elevation measurements acquired by the Mercury Laser Altimeter (MLA) on the MErcury Surface, Space ENvironment, GEochemistry, and Ranging (MESSENGER) mission accurately determine the shape of Mercury's northern hemisphere [2], but MESSENGER's eccentric orbit, with a periapsis at a high northern latitude, placed most of the southern hemisphere beyond MLA's maximum range. Occultations by Mercury of MESSENGER's radio frequency (RF) transmissions [3] provide several hundred measurements of Mercury's radius in the southern hemisphere (Fig. 1). Stereo analyses of images are another source of southern-hemisphere elevations, but the absolute elevations produced from stereo methods are sensitive to small errors in camera geometry.

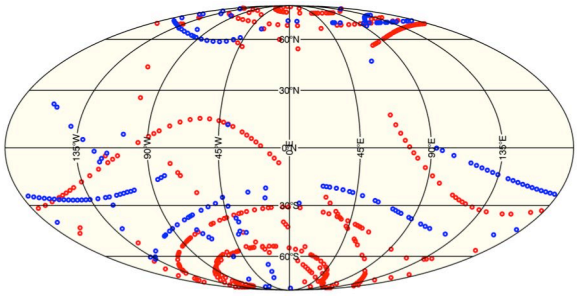

Fig. 1. Location of the occultation measurements used to determine Mercury's long-wavelength shape. Recent data (blue symbols) improve the coverage in the southern hemisphere.

Occultation analysis: The RF path between the known position of MESSENGER and the observing antenna on Earth at the time corresponding to an occultation defines a line, which yields the radius of Mercury at the tangent point of a smooth sphere that is centered at Mercury's center of mass (COM). We fit the predicted diffraction pattern of the RF signal to the received RF power history to identify the time of occultation. Local topography can displace the occultation location both radially and horizontally from the smooth-sphere tangent point. We corrected for these displacements with a stereo photoclinometry (SPC) [4] digital terrain model (DTM) that has sufficient accuracy to identify the occulting feature (Fig. 2). We adjusted the raw occultation radius downward by the height of the feature relative to the average elevation of the surrounding terrain.

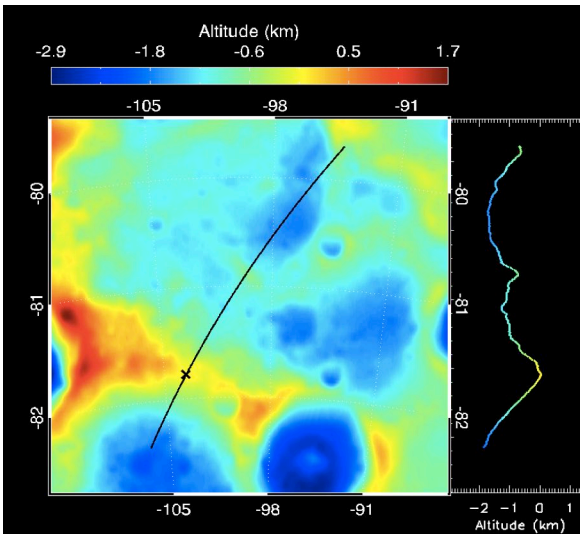

Fig. 2. The RF path (black line) at the time of an occultation overlaid onto an SPC DTM. The terrain model provides the location of the occulting edge and the adjustment required to associate the height of that edge with the elevation of the surrounding terrain. The **x** indicates the occulting edge. The altitude profile along the RF path is shown to the right.

We validated the occultation results by comparing them to MLA measurements in locations where the two datasets overlap. The average difference between the

occultation measurements and the MLA occulting edges was 4±25 m, and the standard deviation in the relative difference was 150 m, in agreement with the average time-based uncertainty of the occultation radii. The average difference for the SPC DTM that was used for topography adjustments of the occultation elevations was 130±30 m with a standard deviation of 330 m. Investigation of the SPC and MLA DTMs showed that the cause of the discrepancy is suppression of the height of crater rims in the SPC DTM. We translated the results of these comparisons to the southern hemisphere and increased the topography adjustment by 130 m and the uncertainty to 330 m.

Mercury's low-degree shape: We expanded MLA and occultation data in spherical harmonics through degree and order 128 (Fig. 3) and found that Mercury's mean radius is 2439.36±0.03 km [5]. The offset between the planet's COM and center of figure (COF) is negligible (40±40 m) along the polar axis and modest (140±50 m) in the equatorial plane. The small offset is consistent with a large core and limited hemispherical asymmetry in crustal thickness.

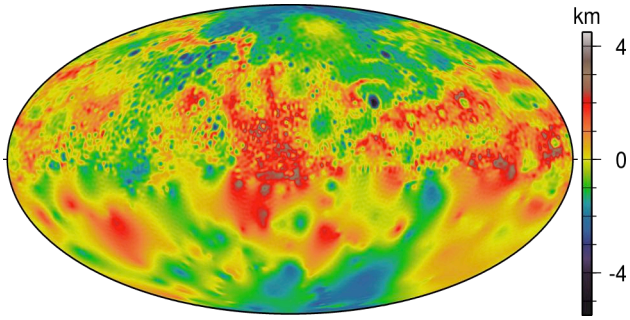

Fig. 3.The shape of Mercury from a damped, spherical harmonic fit to the MLA and occultation data. The sparse coverage of occultations results in lower resolution in the southern hemisphere. The elevations are relative to 2440 km.

Mercury is more oblate than predicted by hydrostatic equilibrium [3, 6]. Mercury's spherical-harmonic shape spectrum is dominated by degree 2 (Figure 4), and the planet's first-order shape is that of a triaxial ellipsoid with semimajor axes *a*, *b*, and *c*. The polar radius, *c,* is 1.65 km less than (*a*+*b*)/2, and the equatorial difference, *a*-*b,* is 1.25 km. Within the 2° uncertainty of the measurement, Mercury's short axis is aligned with its rotation axis. Mercury's long axis is rotated 15° west of Mercury's dynamically defined principal axis, the principal semi-major axis of the mass distribution.

Discussion: Simple pressure balance, a first-order approximation to spherical isostasy, requires a crust that is ~25 km thicker at the equator than the poles. However, such a configuration fails to satisfy the observed second-degree geoid. In fact there is no single-mode density model that will simultaneously satisfy both the degree-2 shape and geoid. What is required is a mixing of high and low "admittance reservoirs" [7], where "admittance" is the spectral ratio of geoid to shape. The crust-mantle boundary of Mercury produces low admittance, and its buoyancy could explain the shape. The same is true of the upper mantle portion of subsurface density anomalies induced by the heterogeneous surface temperature distribution (with hot, cold, and rotational temperature poles) [8, 9]. The buoyancy of lower-mantle density anomalies largely deforms the core-mantle boundary (CMB).

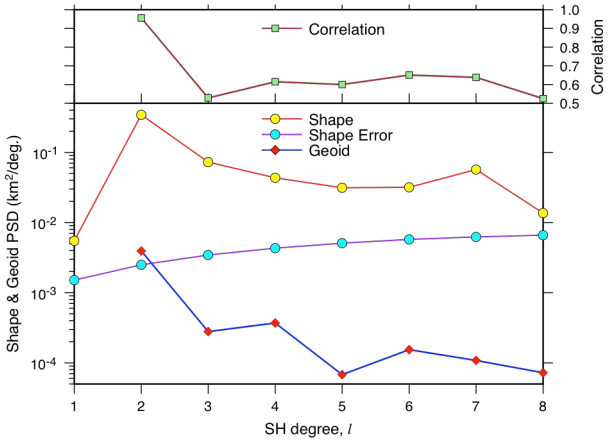

Fig. 4. Power spectral density for Mercury's shape and geoid and the correlation between the two, which is particularly high at degree 2. The errors in the shape are lower bounds.

The upper mantle thermal buoyancy satisfies the observation that the degree-2 geoid and shape are highly correlated (0.99) [3] but requires an accompanying high admittance source, for which a deep density anomaly or a surface load on an elastic lithosphere are obvious candidates. However, we have been unable to identify a plausible deep mantle or CMB degree-2 density source. A surface load can produce a high admittance largely through support by elastic membrane stresses. Indeed, Tosi et al. [9] showed that such a model could satisfy the ensemble of observational constraints provided the elastic lithosphere thickness was between 110 and 180 km thick, which would imply that Mercury was captured into a 3:2 spin orbit resonance more than a billion years after its formation. Finally, we note that in-phase crustal thickness variations may have been generated by partial melting variations related to the surface temperature distribution.

References: [1] Mazarico E. et al. (2014) *JGR Planets*, *119*, 2417. [2] Zuber M.T. et al. (2012) *Science, 336*, 217. [3] Perry M.E. et al. (2015) *GRL*, *42*, 6951. [4] Gaskell, R.W. et al. (2008) *Meteorit. Planet. Sci*., *43*, 1049. [5] Neumann G.A. et al. (2016) *LPS, 47*, this mtg. [6] Matsuyama I. and Nimmo F. (2009) *JGR Planets, 114,* E01010. [7] Chen E. et al. (2015) *AGU Fall Meeting*, P41F-07. [8] Phillips R.J. et al. (2014) *LPS, 45*, 2634. [9] Tosi N. et al. (2015) *GRL, 42,* 7327.